



Design of 3D *h*-BN architecture as Ag₃VO₄ enhanced photocatalysis stabilizer and promoter



Xiaomeng Lv^{a,*}, Jiaxi Wang^a, Zaoxue Yan^a, Deli Jiang^a, Jun Liu^{b,*}

^a School of Chemistry and Chemical Engineering, Jiangsu University, Zhenjiang 212013, PR China

^b School of the Environment and Safety Engineering, Jiangsu University, Zhenjiang 212013, PR China

ARTICLE INFO

Article history:

Received 22 September 2015

Received in revised form 8 March 2016

Accepted 24 March 2016

Available online 30 March 2016

Keywords:

3D *h*-BN

Dielectric

Photocatalytic stabilizer

h-BN/Ag₃VO₄ composite

ABSTRACT

Hexagonal boron nitride (*h*-BN), with a band gap of ~5.5 eV, is commonly excluded photocatalysis and photovoltaic conversion application. Herein, we rationally designed 3D *h*-BN hierarchical architecture with an interconnected network of graphene-analogue *h*-BN nanosheets and wrapped Ag₃VO₄ by *in-situ* precipitation at room temperature. After hybridization, stabilized Ag₃VO₄ with enhanced photocatalytic activity was obtained and the enhanced activity was fluctuated by the varied addition of *h*-BN. The 3 wt% *h*-BN/Ag₃VO₄ composite exhibited the highest photocatalytic activity for the degradation of RhB under visible light, which was 6.2 times that of bare Ag₃VO₄. Meanwhile, it showed higher photocurrent responses, which was about 4 times that of pure Ag₃VO₄. More interestingly, their absorbance intensity were enhanced obviously both in visible and UV light region after hybridization. Structure characterization, as well as the radical trapping experiments were further explored to reveal mechanism of the enhanced activity and stability of *h*-BN/Ag₃VO₄ composite. The results provided an alternative simple and convenient route to stabilize photocatalysts prone to photocorrosion with enhanced performance.

© 2016 Elsevier B.V. All rights reserved.

1. Introduction

In the past few decades, with the rapid development of increasing population and industry, the energy crisis and environmental pollution have become increasingly serious and threaten both human life and the eco-system [1,2]. Semiconductor photocatalysis has drawn much attention as a promising technique for their excellent potential in addressing these issues under abundant solar light [3,4]. Among the traditional semiconductors, TiO₂ and ZnO have been used widely for the degradation of organic dyes due to its low cost, non-toxicity, wide availability and chemical stability [5–7]. However, the inherent feature of the wide band gap limits its photocatalytic efficiency under solar light irradiation [8,9]. Therefore, exploring the visible-light-driven photocatalysts plays a critical role in practical photocatalysis application for the social requirement.

Recently, silver-based semiconductor materials have drawn much attention for the degradation of organic pollutants or splitting water in the field of environmental photocatalysis, such as AgI [10], Ag₃PO₄ [11–13], Ag₂CO₃ [14,15], Ag₃AsO₄ [16], Ag₃VO₄

[17], etc. These promising and sensitive photocatalysts showed photocatalytic activity for the degradation of organic pollutants and splitting water under visible light irradiation for its narrow gap. However, due to the photocorrosion and high recombination of photogenerated electron-hole pairs, they showed poor stability and low photocatalytic activity in the photocatalytic process, which greatly limited their practical application for the degradation of organic dyes. Thereafter, many efforts have been made to improve their stability and activity. As far as Ag₃VO₄ is concerned, modification on its surface or construction of heterojunction with other semiconductors has been reported, such as NiO/Ag₃VO₄ [18], Gd₂O₃/Ag₃VO₄ [19], La₂O₃/Ag₃VO₄ [20], Co₃O₄/Ag₃VO₄ [21], CaFe₂O₄/Ag₃VO₄ [22], Ag₃VO₄/ZnO [23,24], g-C₃N₄/Fe₃O₄/Ag₃VO₄ [25], ZnO/Ag₃VO₄/Fe₃O₄ [26], Ag₃VO₄/TiO₂/graphene [27], Ag₃VO₄/AgBr/Ag [28], g-C₃N₄/Ag₃VO₄ [29–31] and BiOI/Ag₃VO₄ [32], etc. Yet, few investigations shed light on utilizing two-dimensional dielectric materials.

Hexagonal boron nitride (*h*-BN), a structural analogue of graphene, is well known as dielectric material with a band gap of 5–6 eV exhibiting high thermal and chemical stability [33–36]. However, theoretical calculations have demonstrated that the B–N bond was partially ionic, and a slight buckling appeared on the curled surface. Hence, the electronic properties of low-dimensional *h*-BN systems differed considerably from those of bulk *h*-BN and the band gap of monolayer *h*-BN can be considerably

* Corresponding authors.

E-mail addresses: laiyangmeng@163.com (X. Lv), liujun1227@mail.ujs.edu.cn (J. Liu).

reduced by vacancy and impurity defects [37,38]. Furthermore, support effects can significantly modulate the band gap in two-dimensional nanostructures, such as *h*-BN/TiO₂ and *h*-BN/ZnO composite photocatalysts [39,40], Au nanoparticle-loaded TiO₂ with *h*-BN nanosheet [41], introduction of *h*-BN with AgBr and Ag₃PO₄ [42,43]. These properties enlarged the interaction between *h*-BN and semiconductors on the curled surface, leading to hybrid photocatalyst with enhanced activity. More interestingly, designing *h*-BN porous sheets with richly exposed (002) plane edges leads to wide spectrum light absorption in both UV and visible light ranges [44]. Hence, graphene-analogue *h*-BN, as a dielectric material, can be engineered as support in photocatalytic application.

Herein, 3D *h*-BN with exposed (002) plane was synthesized and designed as stabilizer of Ag₃VO₄ with enhanced photocatalysis by *in situ* precipitation method at room temperature. The photocatalytic performance of *h*-BN/Ag₃VO₄ hybrid nanocomposites was investigated by the degradation of Rhodamine B (RhB) under visible light irradiation. Compared with pure Ag₃VO₄, the as-obtained *h*-BN/Ag₃VO₄ photocatalysts showed remarkably enhanced photocatalytic activity and stability towards the degradation of RhB, owing to the higher photocurrent responses, the enhanced absorbance intensity and the improved active species. Furthermore, the possible mechanism for the enhanced photocatalytic activity of *h*-BN/Ag₃VO₄ composite materials was discussed and the stabilization effect of 3D *h*-BN was further explored.

2. Experimental

2.1. Materials

Boric acid (H₃BO₃), Urea (CO(NH₂)₂), Silver nitrate (AgNO₃), Sodium orthovanadate dodecahydrate (Na₃VO₄·12H₂O) and other chemicals were purchased from Sinopharm Chemical Reagent Co., Ltd. All the reagents were of analytical grade and used as received without further purification.

2.2. Synthesis of 3D boron nitride (*h*-BN)

In a typical procedure, boric acid and urea with a molar ratio of 1:24 were fully dissolved in 60 mL of deionized water, dried at 65 °C until the evaporation of water was complete. The dried mixtures were heated at 900 °C for 5 h in a N₂ atmosphere at tubular furnace and *h*-BN was obtained in the form of white powder. The excessive urea played an important role in forming 3D *h*-BN architecture. During the calcination process, gaseous species were liberated, including CO₂, HCNO, H₂O and NH₃. The escape of gases acted as fugitive templates of the final porous structure [45,46].

2.3. Preparation of *h*-BN/Ag₃VO₄ photocatalysts

The *h*-BN/Ag₃VO₄ composites were prepared by precipitation method. Typically, 0.018 g *h*-BN was dispersed in 20 mL of deionized water by ultrasonication for 0.5 h. Then, 0.6972 g AgNO₃ was added into the solution under magnetic stirring for 0.5 h. Next, 20 mL Na₃VO₄ solution (including 0.5474 g Na₃VO₄·12H₂O) was slowly dropped into the mixture solution and reacted under magnetic stirring for 4 h at room temperature in the dark. Finally, the product was centrifugated and washed with deionized water and ethanol for several times and dried under vacuum at 60 °C for 12 h. The sample was named as 3 wt% *h*-BN/Ag₃VO₄ and other *h*-BN/Ag₃VO₄ composites were prepared with different *h*-BN content by the similar method.

2.4. Characterization

The crystal structure and morphology of the prepared products were characterized by a power X-ray diffraction (XRD) (Bruker AXS Company, Germany) using Cu-K α ($\lambda = 1.5406 \text{ \AA}$) radiation at a scanning rate of 7° min⁻¹ in the 2θ range from 10 to 80°. The structure information of samples was analyzed by Fourier Transform Infrared (FT-IR) spectra using a Nexus FT-IR spectrophotometer (Thermo Nicolet, America). Transmission electron microscopy (TEM) was conducted with a JEM-2100 electron microscope (JEOL, Japan) at a 200 kV accelerating voltage. Scanning electron microscopy (SEM) was performed with a scanning electron microscope (JSM-7100F) at an accelerating voltage of 10 kV to investigate the morphology and surface roughness of the samples and Energy-dispersive X-ray spectroscope (EDS) was demonstrated for the elements of the sample. UV-vis diffuse reflectance spectra (DRS) were characterized by a Shimadzu UV-2600 spectrophotometer with BaSO₄ as the reference standard. The Brunauer–Emmett–Teller (BET) specific surface area and pore volume of the samples were obtained by N₂ absorption at 77 K with a NOVA2000e analytical system made by Quantachrome Corporation (USA). The photoluminescence (PL) spectra was measured on Hitachi F-2500 fluorescence spectrophotometer at an excitation wavelength of 362 nm.

2.5. Photocatalytic activity measurement

The photocatalytic activities of as-prepared photocatalysts were assessed by degradation of Rhodamine B (RhB) solution under visible light irradiation using 300 W tungsten lamp equipped with a 420 nm cut-off filter (the reaction temperature was kept at 25 °C by circulating water outside the reaction). In the experiment, 60 mg photocatalysts were poured into 60 mL RhB solution (10 mg/L) in a photoreactor bottle. Before light irradiation, the suspensions were magnetically stirred for 0.5 h to ensure the establishment of absorption-desorption equilibrium in the dark. At given time intervals of visible-light irradiation, 5 mL of solution was collected and centrifuged to remove the catalyst samples, then determined by UV-vis spectrophotometer at the maximum absorption wavelength of RhB at 554 nm. To estimate the stability of the photocatalyst, the used photocatalyst was collected and washed with deionized water and ethanol by centrifugation, then dried for the next degradation of RhB solution and XRD characterization.

2.6. Photoelectrochemical measurements

The photocurrent was carried out by electrochemical station (CHI 660B Chenhua Instrument Company) in a standard three-electrode system. A platinum wire and a saturated calomel electrode were used as counter electrode and reference electrode, respectively. A 500 W Xe lamp was served as the light source. A 0.5 M Na₂SO₄ aqueous solution was utilized as the electrolyte. Working electrode was prepared as follows: 2 mg of sample, 1 mL of ethylene glycol and 10 μL of Nafion were mixed to form homogeneous slurry. The resultant slurry was drop-casted onto a pre-cleaned FTO glass electrode and dried at 60 °C for 12 h.

3. Results and discussion

3.1. XRD analysis

The XRD patterns of as-synthesized samples were shown in Fig. 1. The main diffraction peaks of Ag₃VO₄ were completely in accord with the Ag₃VO₄ monoclinic phase (JCPDS card no. 45-0543) [27]. The diffraction peaks at 2θ values of 19.3°, 31.0°, 32.4°, 34.3°, 35.1°, 36.0°, 39.1°, 41.3°, 48.3°, 51.3° and 54.1° were well corresponded to (001), (-121), (121), (220), (301), (202), (022), (320),

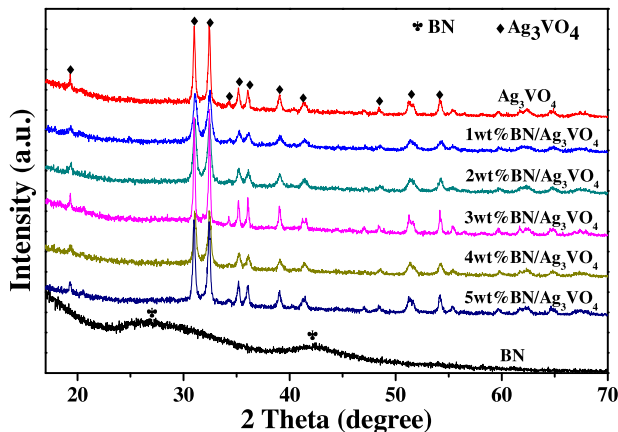


Fig. 1. XRD patterns of *h*-BN, Ag_3VO_4 and *h*-BN/ Ag_3VO_4 composites.

(−322), (132) and (331) planes of monoclinic Ag_3VO_4 , respectively. The wide diffraction peaks at 2θ value of 26.8° and 42.3° were assigned to (002) and (100) planes of hexagonal structure *h*-BN (JCPDS card no. 85-1068) [47]. However, no diffraction peaks of *h*-BN were indicated in the diffraction patterns of *h*-BN/ Ag_3VO_4 composites for its relatively low amount. No impurity diffraction peaks except that of *h*-BN/ Ag_3VO_4 composites were observed, which demonstrated that no other species were obtained during the experiment.

3.2. TEM and SEM analysis

The morphologies and microstructures of as-prepared samples were investigated by TEM and SEM in Figs. 2 and S1. As shown in Fig. S1a, *h*-BN displayed few-layer stacking sheets and large smooth surface, which was a typical character of graphene-like nanosheets structure [48]. Fig. 2a displayed the wrinkled structure of 3D *h*-BN hierarchical architecture assembled by ultrathin *h*-BN nanosheets. Figs. S1b and S1c showed that the pure Ag_3VO_4 sample displayed

irregular nanoparticle structure with an average size of 40–50 nm. After hybridization, Ag_3VO_4 nanoparticles were distributed and wrapped by *h*-BN (Fig. 2b and c). Seen from the HRTEM image in Fig. 2d, the lattice interlinear spacing of 0.34 nm corresponded to the (002) plane of *h*-BN and the interplanar spacing of 0.224 nm, 0.233 nm and 0.248 nm matched with the (400), (022) and (301) plane of Ag_3VO_4 , respectively. For common layered materials, the dominated exposed planes were usually (002) planes, and the (002) plane edge may show higher affinity for gas molecule and/or electrolyte ion adsorption, which was important for their applications in transistors, photovoltaic devices or as photocatalysis materials [44]. Hence, the cross-linked microstructure was formed between *h*-BN and Ag_3VO_4 with exposed (002) plane possessed potential application in photocatalysis. Additionally, the EDS spectra of 3 wt% BN/ Ag_3VO_4 composite was shown in Fig. S1d, which confirmed only existence of the elements B, N, Ag, V, O.

3.3. XPS analysis

The XPS was further employed to analyze the surface elemental composition and chemical state of the sample. Fig. 3a shows the XPS survey scan spectra of the as-prepared 3 wt% *h*-BN/ Ag_3VO_4 composite, specifying the co-existence B, N, Ag, V and O elements without any other impurities, which was consistent with the EDS result. Fig. 3b shows the high-resolution XPS spectra of B 1s. The peak at 190.5 eV in B 1s spectra was ascribed to B–N bonds [49]. The peak at 398.2 eV in N 1s spectrum (Fig. 3c) was assigned to N^{3-} in BN layers [50,51]. The peaks of $\text{Ag} 3d_{3/2}$ and $\text{Ag} 3d_{5/2}$ binding energies were found at 374 eV and 368.1 eV in Fig. 3d, which can be attributed to Ag^+ in Ag_3VO_4 [52]. The two peaks at 516.3 eV and 524 eV were separately assigned to $\text{V} 2p_{5/2}$ and $\text{V} 2p_{3/2}$ binding energies of V^{5+} in Ag_3VO_4 (Fig. 3e) [53]. The peak located at 529.7 eV corresponded to the O 1s binding energy in Fig. 3f. The results revealed the successful preparation of chemical-coupling *h*-BN/ Ag_3VO_4 composites.

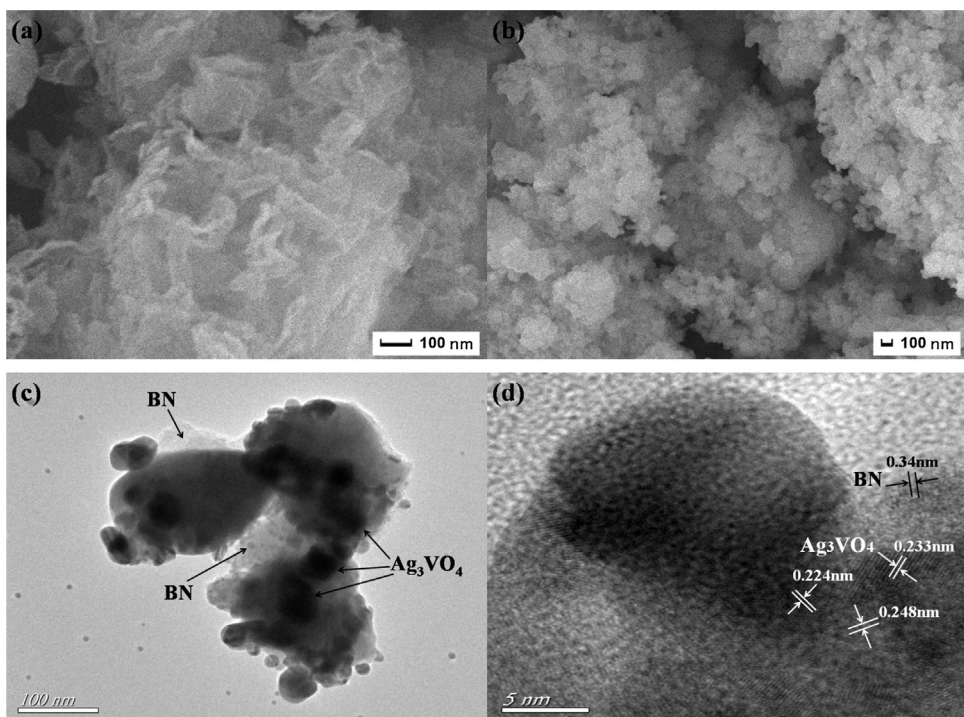


Fig. 2. SEM images of (a) *h*-BN, (b) 3 wt% *h*-BN/ Ag_3VO_4 ; TEM image of (c) 3 wt% *h*-BN/ Ag_3VO_4 and (d) HRTEM image of 3 wt% *h*-BN/ Ag_3VO_4 .

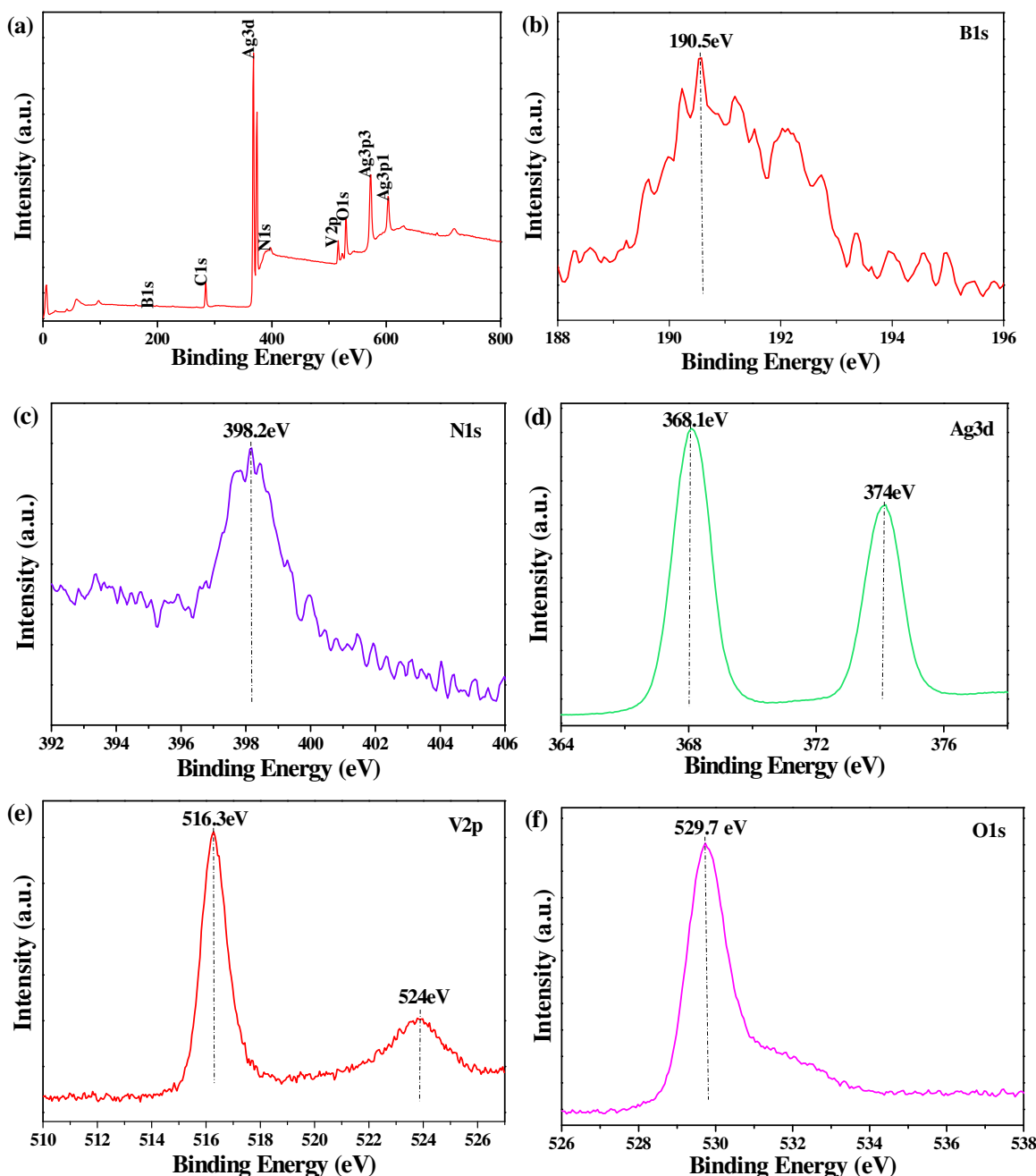


Fig. 3. XPS spectra of 3 wt% *h*-BN/Ag₃VO₄ composite: (a) the survey scan, (b) B 1s, (c) N 1s, (d) Ag 3d, (e) V 2p, (f) O 1s.

3.4. FT-IR analysis

The FT-IR spectra of *h*-BN and *h*-BN/Ag₃VO₄ composites are illustrated in Fig. 4. For FT-IR spectra of *h*-BN, the two absorption peaks at 1387 cm⁻¹ and 805 cm⁻¹ were assigned to the in-plane B–N stretching vibration and out-of-plane B–N–B bending vibration, respectively [54,55]. For FT-IR spectra of Ag₃VO₄, the absorption peaks at 920 cm⁻¹ and 875 cm⁻¹ were corresponded to the V=O double bond vibration and the absorption peak at 687 cm⁻¹ was assigned to the symmetry stretching vibration of V–O–V units [56,57]. The sharp and broad absorption peaks at 1631 cm⁻¹ and 3150–3500 cm⁻¹ were assigned to the δ(O–H) bending vibration and ν(O–H) stretching vibration for the absorbed H₂O on the surface of samples, respectively. In the case of *h*-BN/Ag₃VO₄ composites, the absorption peak of *h*-BN at 1387 cm⁻¹

was observed obviously and the absorption intensity was enhanced with the increasing of *h*-BN content. Additionally, new peak in ~1400 cm⁻¹ appeared after hybridization, indicating that *h*-BN was successfully interconnected with Ag₃VO₄.

3.5. N₂ adsorption-desorption studies

The higher specific surface area is an important factor for the photodegradation of dyes, which can support more active sites and has higher adsorption capacity in the photocatalytic reaction [58,59]. N₂ adsorption-desorption isotherm curves and the pore size distribution plots (inset) of pure Ag₃VO₄ and 3 wt% *h*-BN/Ag₃VO₄ were analyzed by the BET calculation model and BJH model in Fig. 5. The BET specific surface area of pure Ag₃VO₄ and 3 wt% *h*-BN/Ag₃VO₄ was 27.09 m²/g and 32.75 m²/g, respectively.

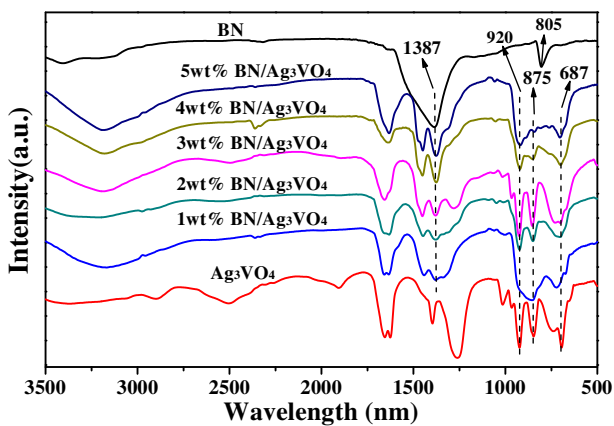


Fig. 4. FT-IR spectra of the as prepared samples.

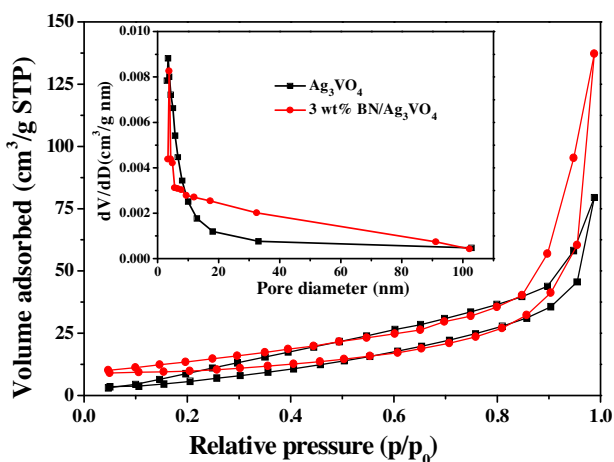


Fig. 5. N_2 adsorption-desorption isotherm curves and pore size distributions (inset) of pure Ag_3VO_4 and 3 wt% BN/ Ag_3VO_4 .

Additionally, the pore volume was $0.127\text{ cm}^3/\text{g}$ and $0.202\text{ cm}^3/\text{g}$, respectively, and the pore diameter was 3.46 nm and 3.78 nm , respectively. The results indicated that the physical property of 3 wt% h-BN/ Ag_3VO_4 was engineered by the introduction of h-BN, which can improve the adsorption capacity and provide more reactive sites and that might contribute to the enhancement of photocatalytic activity.

3.6. Optical absorption property

The optical properties of the as-prepared samples were investigated using UV-vis diffuse reflectance spectroscopy, which determined the band gap of the samples. Fig. S2 shows the UV-vis diffuse reflectance spectra of pure Ag_3VO_4 and h-BN/ Ag_3VO_4 composites. It is known that h-BN has no optical absorption in a wavelength range of 300–800 nm. However, pure Ag_3VO_4 can work over the whole above spectrum. After hybridization, the absorbance intensity of h-BN/ Ag_3VO_4 composites was enhanced obviously both in visible and UV light region and the red shift in the visible light region was also found, which suggested that the recombination process of photoinduced electron-hole pairs can be restrained and the photocatalytic activity of BN/ Ag_3VO_4 composites can be excessively improved with increasing small amount of h-BN [60].

3.7. Photocatalytic activity and stability of the samples

The photocatalytic activity of h-BN/ Ag_3VO_4 composites with different contents of h-BN was evaluated by the photocatalytic degradation of RhB solution under visible light irradiation after the adsorption-desorption equilibrium. Fig. 6a shows the temporal evolution of the spectral change of RhB solution by 3 wt% h-BN/ Ag_3VO_4 under different visible light irradiation time. The absorption peak of RhB solution at 554 nm decreased quickly and the maximum absorption wavelength displayed a gradual blue shift with increasing irradiation time, which demonstrated that the chromophoric structure of the ethyl groups of RhB was decomposed step-by-step [61]. The color of RhB solution changed from red to colorlessness, indicating that RhB dye was almost degraded in 75 min. As can be clearly seen from Fig. 6b, the RhB solution was hardly degraded under visible light irradiation without the photocatalyst, which indicated that RhB was stable and difficult to be decomposed. After 90 min of visible light irradiation, only 44% of RhB solution was degraded over the pure Ag_3VO_4 . All the h-BN/ Ag_3VO_4 composites showed higher photocatalytic activity than pure Ag_3VO_4 , which suggested that the amount of BN had a significant effect on the photocatalytic performance of h-BN/ Ag_3VO_4 . As the amount of h-BN increased to 3 wt%, the h-BN/ Ag_3VO_4 with BET surface area of $32.75\text{ m}^2/\text{g}$ exhibited the highest photocatalytic degradation rate of 96.3% for RhB solution, which was 2.19 times that of pure Ag_3VO_4 with BET surface area of $27.09\text{ m}^2/\text{g}$. However, the photocatalytic performance of h-BN/ Ag_3VO_4 had a slight decrease with increasing of h-BN amount. It was suggested that excess h-BN contents in the composites were unfavorable and the active site of Ag_3VO_4 may be covered by higher content of h-BN, thereby the electron transfer efficiency of the photoinduced electrons from Ag_3VO_4 nanoparticles to h-BN surfaces were decreased [42,60]. Hence, the enhancement of photocatalytic activity of h-BN/ Ag_3VO_4 composites were attributed to the significant synergistic effect between graphene-like h-BN and Ag_3VO_4 , which can have an important role in the separation of the photoinduced electron-hole pairs.

To further understand the photocatalytic reaction kinetics of the RhB degradation, a pseudo-first-order reaction model was used to describe the experimental result as Eq. (1)

$$\ln(C/C_0) = -k_{app}t \quad (1)$$

where, C was the RhB concentration at the reaction time t , C_0 was the initial concentration of RhB, k_{app} was the apparent pseudo-first-order reaction rate constant (min^{-1}). The pseudo-first-order kinetics rates of RhB photocatalytic degradation are displayed in Fig. 7 and the reaction rate constant k_{app} is listed in Table S1. It could be clearly seen that the RhB photocatalytic degradation reaction had a good linear relationship with pseudo-first-order reaction kinetics and the kinetic rate constant k_{app} of h-BN/ Ag_3VO_4 composite were higher than that of the pure Ag_3VO_4 under visible light irradiation. When the h-BN content was up to 3 wt%, the RhB photocatalytic degradation rate constant k_{app} of the composite was 0.0384 min^{-1} , which was 6.2 times that of pure Ag_3VO_4 (0.0062 min^{-1}). In order to further investigate the photocatalytic performance of h-BN/ Ag_3VO_4 composite, the other dye pollutants of MB and MO solution were evaluated under the same condition. As shown in Fig. S3, it could be seen that 93.5% of MB and 87.1% of MO were degraded by 3 wt% h-BN/ Ag_3VO_4 composite after 95 min under visible light irradiation. As comparison, only 36.8% of MB and 32.2% of MO were decomposed by pure Ag_3VO_4 . The comparison experimental results also indicated that the photocatalytic activity of h-BN/ Ag_3VO_4 composite was much higher than that of pure Ag_3VO_4 . Furthermore, the enhanced activity indicated that the photoinduced electrons and holes of photocatalytic composites can be efficiently separated

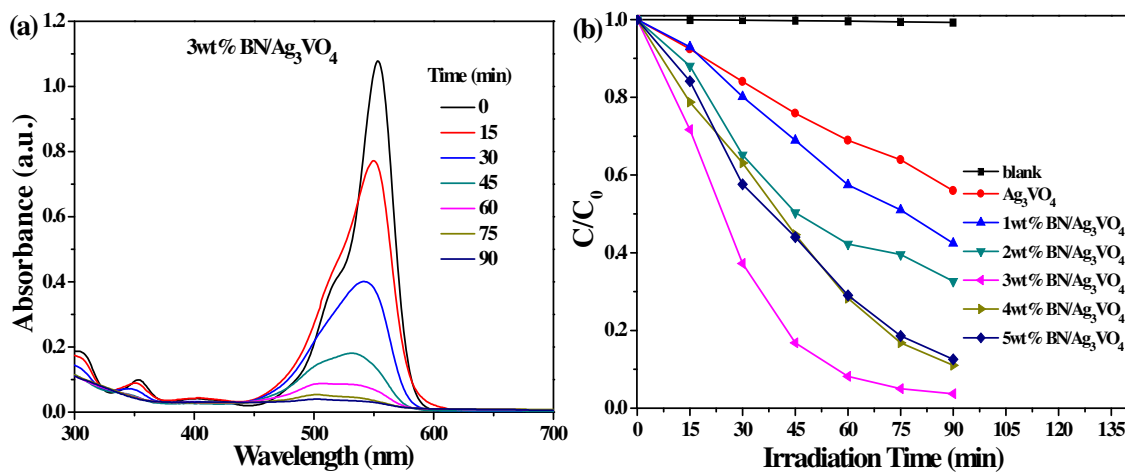


Fig. 6. Absorption spectra of RhB solution with different time by 3 wt% *h*-BN/Ag₃VO₄ photocatalyst (a); Photocatalytic degradation of RhB solution over the pure Ag₃VO₄ and *h*-BN/Ag₃VO₄ composites under visible light irradiation (b).

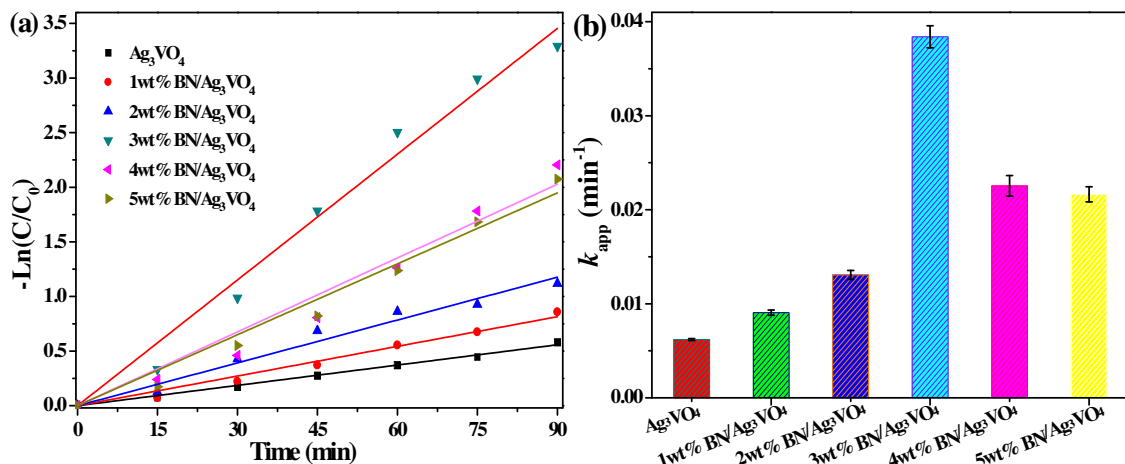


Fig. 7. Pseudo-first-order kinetics rates of photocatalytic degradation of RhB by Ag₃VO₄ and *h*-BN/Ag₃VO₄ composites (a); the reaction rate constant k_{app} of the samples (b).

and the photocatalytic activity can be remarkably enhanced by the addition of *h*-BN.

The stability and recyclability of the photocatalysts were extremely important factor for practical applications. To investigate the stability and recyclability of 3 wt% *h*-BN/Ag₃VO₄ composite, five successive cycling runs for the photodegradation of RhB were performed and the results are shown in Fig. S4a. It could be seen clearly that the photocatalytic activity of 3 wt% *h*-BN/Ag₃VO₄ for the RhB degradation only slightly decreased and the degradation rate still remained over 90% after five cycles under visible light irradiation, which indicated that the *h*-BN/Ag₃VO₄ composite was chemically stable. In addition, the XRD patterns of 3 wt% *h*-BN/Ag₃VO₄ composite before and after five recycling runs for the photocatalytic reaction are shown in Fig. S4b. It could be seen that no new peak of Ag was observed in the composite, which confirmed that BN played a significant role in stabilizing the composites.

3.8. PL and photocurrent analysis

It is known that the recombination of electrons and holes has a great influence on the photocatalytic activity. The recombination rate of photo-generated electrons and holes in semiconductors was investigated by PL emission technique. Generally, the higher fluorescence intensity indicated the more recombination of the

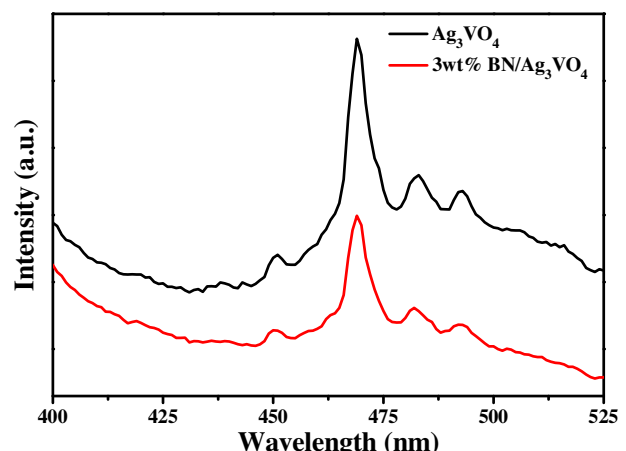


Fig. 8. Photoluminescence (PL) spectra of Ag₃VO₄ and 3 wt% *h*-BN/Ag₃VO₄.

photo-generated carriers and lower photocatalytic activity [31,62]. Fig. 8 shows the similar PL spectra of the pure Ag₃VO₄ and 3 wt% *h*-BN/Ag₃VO₄ under the excitation wavelength at 362 nm. However, the intensity of emission peak of composites decreased significantly, which distinctly demonstrated that the 3 wt% *h*-BN/Ag₃VO₄ exhibited lower recombination ability of photo-generated carriers.

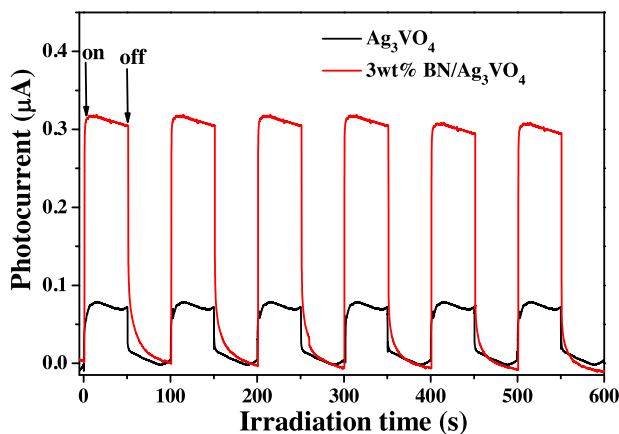


Fig. 9. Transient photocurrent responses of the pure Ag_3VO_4 and 3 wt% $h\text{-BN}/\text{Ag}_3\text{VO}_4$.

The result clearly indicated that the presence of $h\text{-BN}$ can improve the separation efficiency of photo-generated electron-hole pairs and enhance the corresponding photocatalytic activity.

To further evaluate charge transfer and separation processes between $h\text{-BN}$ and Ag_3VO_4 , the transient photocurrent responses of the samples were measured for several cycles of on-off under visible light irradiation [63]. Fig. 9 shows the transient photocurrent responses of pure Ag_3VO_4 and 3 wt% $h\text{-BN}/\text{Ag}_3\text{VO}_4$. It was clearly shown that 3 wt% $h\text{-BN}/\text{Ag}_3\text{VO}_4$ composite showed higher photocurrent responses, which was about 4 times that of pure Ag_3VO_4 . The results indicated that the small content of $h\text{-BN}$ can effectively separate the photogenerated electron-hole pairs of Ag_3VO_4 and improve longer lifetime of the photoexcited charge carriers during the photocatalytic degradation reaction, indicating that the photocatalytic activity of $h\text{-BN}/\text{Ag}_3\text{VO}_4$ can be obviously improved by the addition of $h\text{-BN}$.

3.9. The proposed photocatalytic mechanism

The higher photocatalytic activity and stability of $h\text{-BN}/\text{Ag}_3\text{VO}_4$ composites were obtained after hybridization. In order to further explore the photocatalytic mechanism of 3 wt% $h\text{-BN}/\text{Ag}_3\text{VO}_4$ composite, the main active species during the photocatalytic process for the degradation of RhB were determined by the trapping experiments. Three different quenchers, ammonium oxalate (AO), $t\text{-BuOH}$ and BQ were used as the hole (h^+) scavenger, hydroxyl radical ($\cdot\text{OH}$) scavenger and superoxide radical ($\cdot\text{O}_2^-$), respectively. Fig. 10 shows the degradation of RhB by the 3 wt% $h\text{-BN}/\text{Ag}_3\text{VO}_4$ composite with different scavenges. After $t\text{-BuOH}$ (1 mmol) as hydroxyl radical scavenger was added into the solution [64], the photocatalytic activity of 3 wt% $h\text{-BN}/\text{Ag}_3\text{VO}_4$ for degradation of RhB slightly was not obviously changed (94.4%), indicating $\cdot\text{OH}$ had no influence on the photodegradation of RhB. However, when AO (1 mmol) as hole scavenger was added [65], the photocatalytic activity of 3 wt% $h\text{-BN}/\text{Ag}_3\text{VO}_4$ for degradation of RhB was restrained (12.2%), indicating the h^+ was the prominent active species. Moreover, when BQ (1 mmol) was added as $\cdot\text{O}_2^-$ scavenger [66], the photodegradation of RhB was slightly inhibited (59.6%), indicating $\cdot\text{O}_2^-$ was also involved in the photocatalytic progress. The above results revealed that the photogenerated h^+ and $\cdot\text{O}_2^-$ radical could be the main reaction species in the photocatalytic reaction for the degradation of RhB.

Based on the above experimental results, the mechanism for photocatalytic activity of organic dye towards 3D $h\text{-BN}/\text{Ag}_3\text{VO}_4$ is proposed in Fig. 11. The electron-hole pairs of Ag_3VO_4 photocatalyst were excited under visible light irradiation. The electrons at VB were then transferred to CB, leaving the holes in the VB of

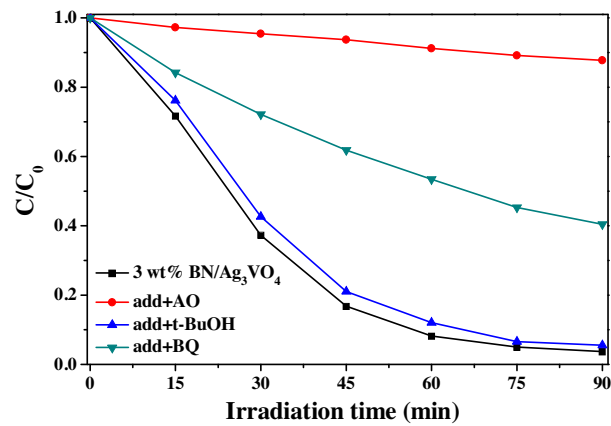


Fig. 10. Photocatalytic degradation of RhB with different scavenges in the presence of 3 wt% $h\text{-BN}/\text{Ag}_3\text{VO}_4$ composite under visible light irradiation.

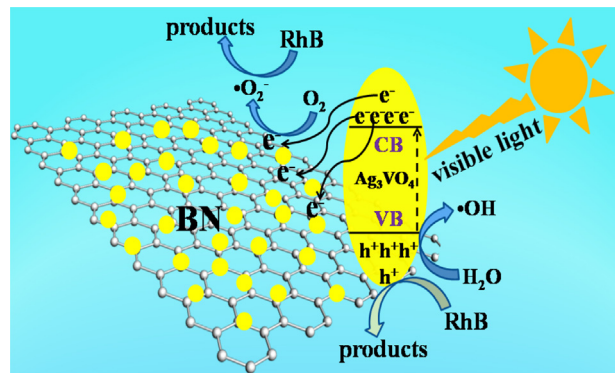


Fig. 11. Proposed mechanism for photocatalytic activity of organic dye over graphene-analogue $h\text{-BN}/\text{Ag}_3\text{VO}_4$ nanocomposite.

Ag_3VO_4 . However, due to the quick recombination of photogenerated electrons and holes, the photocatalytic performance for the degradation of RhB was unsatisfactory. When the $h\text{-BN}$ was coupled with Ag_3VO_4 to form the composite materials, the excited electrons in the CB of Ag_3VO_4 could transfer to the surface of $h\text{-BN}$ for interfacial interaction between Ag_3VO_4 and graphene-analogue $h\text{-BN}$. The effort could effectively suppress the recombination of photogenerated electrons and holes and avoid the photocorrosion of pure Ag_3VO_4 , which finally enhanced the photocatalytic activity and stability for the degradation of RhB. At the same time, the excited electrons on the $h\text{-BN}$ could be trapped to form $\cdot\text{O}_2^-$ with oxygen. Hence, the superoxide radical ($\cdot\text{O}_2^-$) and holes (h^+) were the main oxidation species for the photodegradation of RhB during the photocatalytic reaction, the amount of which were also enhanced after hybridization.

4. Conclusions

In summary, the graphene-analogue $h\text{-BN}/\text{Ag}_3\text{VO}_4$ hybrid photocatalysts were successfully synthesized via *in situ* precipitation method. Compared with pure Ag_3VO_4 , the as-prepared composites showed excellent photocatalytic activity and stability for the degradation of RhB under visible light. The optimum photocatalytic performance of the 3 wt% $h\text{-BN}/\text{Ag}_3\text{VO}_4$ was about 6.2 times higher than those of bare Ag_3VO_4 towards degradation of RhB. The enhancement of photocatalytic activity was ascribed to the synergistic effect owing to the introduction of 3D $h\text{-BN}$, which could not only increase the photocatalytic activity but the stability. More interestingly, the higher photocurrent responses, the enhanced

absorbance intensity, larger BET surface area and more active species of superoxide radical ($\bullet\text{O}_2^-$) and holes (h^+) were obtained. The results provided an alternative simple and convenient route to stabilize photocatalysts prone to photocorrosion with enhanced performance. Also, the present work provides potential application for the graphene-analogue *h*-BN-based photocatalysts in pollutant treatment.

Acknowledgements

We acknowledge the financial supports of the National Natural Science Foundation (Nos. 21003065, 21306067), Jiangsu Province Research Joint Innovation Fund-Perspective Joint Research Project (BY2014123-08) and Natural Science Foundation of Jiangsu (BK20130490).

Appendix A. Supplementary data

Supplementary data associated with this article can be found, in the online version, at <http://dx.doi.org/10.1016/j.molcata.2016.03.036>.

References

- [1] M.A. Al-Ghouti, M.A.M. Khraisheh, S.J. Allen, M.N. Ahmad, *J. Environ. Manage.* 69 (2003) 229–238.
- [2] M.R. Hoffmann, S.T. Martin, W. Choi, D.W. Bahnemann, *Chem. Rev.* 95 (1995) 69–96.
- [3] J. Lee, D.C. Sorescu, X.Y. Deng, *J. Am. Chem. Soc.* 133 (2011) 10066–10069.
- [4] C.L. Yu, J.C. Yu, *Catal. Lett.* 129 (2009) 462–470.
- [5] S.W. Liu, J.G. Yu, M. Jaroniec, *Chem. Mater.* 23 (2011) 4085–4093.
- [6] G. Cappelletti, C.L. Bianchi, S. Ardizzone, *Appl. Catal. B* 78 (2008) 193–201.
- [7] Q. Deng, X.W. Duan, D.H.L. Ng, H.B. Tang, Y. Yang, M.G. Kong, Z.K. Wu, W.P. Cai, G.Z. Wang, *ACS Appl. Mater. Interfaces* 4 (2012) 6030–6037.
- [8] C. Chen, W. Ma, J. Zhao, *Chem. Soc. Rev.* 39 (2010) 4206–4219.
- [9] G. Liu, Y. Zhao, C. Sun, F. Li, G.Q. Lu, H.M. Cheng, *Angew. Chem. Int. Ed.* 47 (2008) 4516–4520.
- [10] C. Hu, T.W. Peng, X.X. Hu, Y.L. Nie, X.F. Zhou, J.H. Qu, H. He, *J. Am. Chem. Soc.* 132 (2010) 857–862.
- [11] Y.P. Bi, H.Y. Hu, S.X. Ouyang, G.X. Lu, J.Y. Cao, J.H. Ye, *Chem. Commun.* 48 (2012) 3748–3750.
- [12] W. Teng, X.Y. Li, Q.D. Zhao, J.J. Zhao, D.K. Zhang, *Appl. Catal. B* 125 (2012) 538–545.
- [13] H.Y. Hu, Z.B. Jiao, C.L. Yu, G.X. Lu, J.H. Ye, Y.P. Bi, *J. Mater. Chem. A* 1 (2013) 2387–2390.
- [14] C.L. Yu, G. Li, S. Kumar, K. Yang, R.C. Jin, *Adv. Mater.* 26 (2014) 892–898.
- [15] J.X. Wang, J.Y. Shen, D.L. Fan, Z.S. Cui, X.M. Lü, *Mater. Lett.* 147 (2015) 8–11.
- [16] J.T. Tang, Y.H. Liu, H.Z. Li, Z. Tan, D.T. Li, *Chem. Commun.* 49 (2013) 5498–5500.
- [17] R. Konta, H. Kato, H. Kobayashi, A. Kudo, *Phys. Chem. Chem. Phys.* 5 (2003) 3061–3065.
- [18] X.X. Hu, C. Hu, *J. Solid State Chem.* 180 (2007) 725–732.
- [19] G.S. Sun, H. Xu, H.M. Li, H.M. Shu, C.T. Liu, Q. Zhang, *React. Kinet. Mech. Catal.* 99 (2010) 471–484.
- [20] H. Xu, H.M. Li, G.S. Sun, J.X. Xie, C.D. Wu, Z.X. Ye, Q. Zhang, *Chem. Eng. J.* 160 (2010) 33–41.
- [21] L. Zhang, Y.M. He, P. Ye, W.H. Qin, Y. Wu, T.H. Wu, *Mater. Sci. Eng. B* 178 (2013) 45–52.
- [22] S.F. Chen, W. Zhao, W. Liu, H.Y. Zhang, X.L. Yu, Y.B. Chen, *J. Hazard. Mater.* 172 (2009) 1415–1423.
- [23] F. Kiantazh, A. Habibi-Yangjeh, *Mater. Sci. Semicond. Process.* 39 (2015) 671–679.
- [24] F. Kiantazh, A. Habibi-Yangjeh, *Solid State Sci.* 49 (2015) 68–77.
- [25] M. Mousavi, A. Habibi-Yangjeh, *Mater. Chem. Phys.* 163 (2015) 421–430.
- [26] M. Shekofteh-Gohari, A. Habibi-Yangjeh, *Solid State Sci.* 48 (2015) 177–185.
- [27] J.X. Wang, P.X. Wang, Y.T. Cao, J. Chen, W.J. Li, Y. Shao, Y. Zheng, D.Z. Li, *Appl. Catal. B* 136–137 (2013) 94–102.
- [28] Q. Zhu, W.S. Wang, L. Lin, G.Q. Gao, H.L. Guo, H. Du, A.W. Xu, *J. Phys. Chem.* 117 (2013) 5894–5900.
- [29] S.Z. Wu, K. Li, W.D. Zhang, *Appl. Surf. Sci.* 324 (2015) 324–331.
- [30] T.T. Zhu, Y.H. Song, H.Y. Ji, Y.G. Xu, Y.X. Song, J.X. Xia, Y. Sheng, Y.P. Li, H. Xu, Q. Zhang, H.M. Li, *Chem. Eng. J.* 271 (2015) 96–105.
- [31] S.M. Wang, D.L. Li, C. Sun, S.G. Yang, Y. Guan, H. He, *Appl. Catal. B* 144 (2014) 885–892.
- [32] S.M. Wang, Y. Guan, L.P. Wang, W. Zhao, H. He, J. Xiao, S.G. Yang, C. Sun, *Appl. Catal. B* 168–169 (2015) 448–457.
- [33] C.R. Dean, A.F. Young, I. Meric, C. Lee, L. Wang, S. Sorgenfrei, K. Watanabe, T. Taniguchi, P. Kim, K.L. Shepard, *Nat. Nanotechnol.* 5 (2010) 722–726.
- [34] L. Song, L.J. Ci, H. Lu, P.B. Sorokin, C.H. Jin, J. Ni, A.G. Kvashnin, D.G. Kvashnin, J. Lou, B.I. Yakobson, *Nano Lett.* 10 (2010) 3209–3215.
- [35] Z. Liu, LL. Ma, G. Shi, W. Zhou, Y.J. Gong, S.D. Lei, X.B. Yang, J.N. Zhang, J.J. Yu, *Nat. Nanotechnol.* 8 (2013) 119–124.
- [36] D.J. Lee, B. Lee, K.H. Park, H.J. Ryu, S. Jeon, S.H. Hong, *Nano Lett.* 15 (2015) 1238–1244.
- [37] C. Ataca, S. Ciraci, *Phys. Rev. B* 82 (2010) 165402–165411.
- [38] A. Nag, K. Raidongia, K.P.S.S. Hembram, R. Datta, U.V. Waghmare, C.N.R. Rao, *ACS Nano* 4 (2010) 1539–1544.
- [39] X.L. Fu, Y.F. Hu, Y.G. Yang, W. Liu, S.F. Chen, *J. Hazard. Mater.* 244–245 (2013) 102–110.
- [40] X.L. Fu, Y.F. Hu, T. Zhang, S.F. Chen, *Appl. Surf. Sci.* 280 (2013) 828–835.
- [41] Y. Ide, F. Liu, J. Zhang, N. Kawamoto, K. Komaguchi, Y. Bando, D. Golberg, *J. Mater. Chem. A* 2 (2014) 4150–4156.
- [42] J.J. Chen, J.X. Zhu, Z.L. Da, H. Xu, J. Yan, H.Y. Ji, H.M. Shu, H.M. Li, *Appl. Surf. Sci.* 313 (2014) 1–9.
- [43] Y.H. Song, H. Xu, C. Wang, J.J. Chen, J. Yan, Y.G. Xu, Y.P. Li, C.B. Liu, Y.C. Lei, *RSC Adv.* 4 (2014) 56853–56862.
- [44] Q.H. Weng, Y. Ide, X.B. Wang, X. Wang, C. Zhang, X.F. Jiang, Y.M. Xue, P.C. Dai, K.J. Komaguchi, Y. Bando, D. Golberg, *Nano Energy* 16 (2015) 19–27.
- [45] D. Liu, W.W. Lei, S. Qin, Y. Chen, *Sci. Rep.* 4 (2014) 4453–4457.
- [46] J.C. Oxley, J.L. Smith, S. Naik, J. Moran, *J. Energy Mater.* 27 (2009) 17–39.
- [47] C.J. Xiong, W.X. Tu, *Eur. J. Inorg. Chem.* 19 (2014) 3010–3015.
- [48] X.F. Yang, J.L. Qin, Y. Jiang, K.M. Chen, X.H. Yan, D. Zhang, R. Li, H. Tang, *Appl. Catal. B* 166–167 (2015) 231–240.
- [49] L. Ci, L. Song, C. Jin, D. Jariwala, D. Wu, Y. Li, A. Srivastava, Z.F. Wang, K. Storr, L. Balicas, P.M. Ajayan, *Nat. Mater.* 9 (2010) 430–435.
- [50] A.S. Nazarov, V.N. Demin, E.D. Grayfer, A.I. Bulavchenko, A.T. Arymbaeva, H.J. Shin, J.Y. Choi, V.E. Fedorov, *Chem.: Asian J.* 7 (2012) 554–560.
- [51] Y. Shi, C. Hamsen, X. Jia, K.K. Kim, A. Reina, M. Hofmann, A.L. Hsu, K. Zhang, H. Li, Z.Y. Juang, *Nano Lett.* 10 (2010) 4134–4139.
- [52] J. Bai, Y.X. Li, M.Y. Li, S.G. Wang, C.Q. Zhang, Q.B. Yang, *Appl. Surf. Sci.* 254 (2008) 4520–4523.
- [53] X. Hu, H.M. Li, L. Xu, C.D. Wu, G.S. Sun, Y.G. Xu, J.Y. Chu, *Ind. Eng. Chem. Res.* 48 (2009) 10771–10778.
- [54] Z.Y. Zhao, Z.G. Yang, Y. Wen, Y.H. Wang, *J. Am. Ceram. Soc.* 94 (2011) 4496–4501.
- [55] C.J. Huang, C. Chen, X.X. Ye, *J. Mater. Chem. A* 1 (2013) 12192–12197.
- [56] D. Chandra, K. Saito, T. Yui, M. Yagi, *Angew. Chem. Int. Ed.* 52 (2013) 12606–12609.
- [57] J.G. Yu, L.F. Qi, M. Jaroniec, *J. Phys. Chem. C* 114 (2010) 13118–13125.
- [58] M. Wang, M.H. Li, L.Q. Xu, L.C. Wang, Z.C. Ju, G.D. Li, Y.T. Qian, *Catal. Sci. Technol.* 1 (2011) 1159–1165.
- [59] Z.F. Jiang, D.L. Jiang, Z.X. Yan, D. Liu, K. Qian, J.M. Xie, *Appl. Catal. B* 170–171 (2015) 195–205.
- [60] S. Kumar, T. Surendar, A. Baruah, V. Shanker, *J. Mater. Chem. A* 1 (2013) 5333–5340.
- [61] J.D. Zhuang, W.X. Dai, Q.F. Tian, Z.H. Li, L.Y. Xie, J.X. Wang, P. Liu, *Langmuir* 26 (2010) 9686–9694.
- [62] L.Q. Jing, Y.C. Qu, B.Q. Wang, S.D. Li, B.J. Jiang, L.B. Yang, W. Fu, H.G. Fu, J.Z. Sun, *Solar Energy Mater. Solar C* 90 (2006) 1773–1787.
- [63] X.M. Lü, J.Y. Shen, J.X. Wang, Z.S. Cui, J.M. Xie, *RSC Adv.* 5 (2015) 15993–15999.
- [64] T.L. Xu, Y. Cai, K.E. O’Shea, *Environ. Sci. Technol.* 41 (2007) 5471–5477.
- [65] W.J. Li, D.Z. Li, W.J. Zhang, Y. Hu, Y.H. He, X.Z. Fu, *J. Phys. Chem. C* 114 (2010) 2154–2159.
- [66] R. Palominos, J. Freer, M.A. Mondaca, H.D. Mansilla, *J. Photochem. Photobiol. A* 193 (2008) 139–145.